OPEN ACCESS
JOURNAL OF ADVANCED DIELECTRICS
Vol. 12, No. 3 (2022) 2250003 (11 pages)

DOI: 10.1142/S2010135X22500035

# Agreement in experimental and theoretically obtained electrocaloric effect in optimized $Bi^{3+}$ doped $PbZr_{0.52}Ti_{0.48}O_3$ material

Shubhpreet Kaur*, Mehak Arora*, Sunil Kumar*, Parambir Singh Malhi†, Mandeep Singh* and Anupinder Singh*,‡

*Department of Physics, Guru Nanak Dev University, Amritsar, 143001 Punjab, India

†Department of Chemistry, Guru Nanak Dev University, Amritsar, 143001 Punjab, India

‡anupinder.phy@gndu.ac.in

Received 2 January 2022; Revised 21 January 2022; Accepted 20 February 2022; Published 9 March 2022

This work harmonizes the experimental and theoretical study of electrocaloric effect (ECE) in $(Pb_{0.8}Bi_{0.2})(Zr_{0.52}Ti_{0.48})O_3$ solid solution by optimizing sintering temperature. $Bi^{3+}$-doped $PbZr_{0.52}Ti_{0.48}O_3$ solid solutions were synthesized by the conventional solid-state reaction method. Different samples were prepared by varying the sintering temperature. X-ray diffraction study confirms the crystalline nature of all the samples. An immense value of polarization has been acquired in the optimized sample. The maximum adiabatic temperature change of order 2.53 K with electrocaloric strength of 1.26 K mm $kV^{-1}$ has been achieved experimentally. Whereas a comparatively close value of ECE has been acquired from the theoretical calculations using a phenomenological approach. Furthermore, a large value (218 mJ $cm^{-3}$) of thermal energy conversion has been obtained using the Olsen cycle.

*Keywords*: Ferroelectrics; solid-state reaction method; electrocaloric effect; energy harvesting.

## 1. Introduction

Over the past decade, the ferroelectric materials have been utilized extensively for technological and scientific applications. Due to their adaptable properties such as ferroelectric, piezoelectric and pyroelectric effects, these materials are used in numerous progressive applications including sensors, transducers and actuators.[1–4] In addition to this, these materials have earned much concern due to the increasing demand of cooling technologies and energy conversion applications.[1,2,4–6]

Owing to the search of efficient solid-state cooling technology and to diminish the expenditure of greenhouse gases which are laboriously used in conventional chilling processes, research in the field of electrocaloric effect (ECE) has experienced quick evolution. The ECE is defined as a mercurial variation in material's temperature under adiabatic conditions upon the application and evacuation of an external electric field. This effect gave rise to great interest in the 1960s onwards,[7–9] but has not been utilized commercially due to small values of reported electrocaloric strength.[7] Ferroelectrics by having net dipole moment exhibits an increase in polarization with the electric field. Moreover, the application of an electric field causes a reduction in entropy leading to an adiabatic increase in temperature in these materials. By considering these concepts, many ferroelectric materials particularly relaxor ferroelectrics have been inquired.[7,8,10–14] Additionally, the dipolar entropy change in ferroelectrics can be calculated by using a standard phenomenological approach.[15,16]

Lead oxide-based materials usually lead zirconate titanate (PZT) have shown the strong experimental, practical and technological significance. Due to high dielectric properties, PZT materials can be employed in various electronic instruments such as nonvolatile memories, modulators, optical shutters, and infrared sensors.[17–19] PZT could be paraelectric, ferroelectric and antiferroelectric depending upon the concentration of Zr.[20] Zr rich PZT ceramics give encouraging ECE due to the pronounced converse effect of pyroelectricity.[21] With the help of appropriate doping at A/B-site, a myriad of compounds have been synthesized.[22] These compounds have been proven to be quite essential for several industrial applications. For specimen, bulk $Pb_{0.99}Nb_{0.02}(Zr_{0.75}Sn_{0.20}Ti_{0.05})_{0.98}O_3$ has exhibited ECE with a peak value of 2.5 K in 750 V.[7] Mischenko *et al.* have reported a temperature change of 0.02°C with 1 kV $mm^{-1}$ at room temperature in $PbZr_{0.95}Ti_{0.05}O_3$ thin films.[11] Recently, a large ECE has been reported in $Pb_{0.92}La_{0.08}(Zr_{0.65}Ti_{0.35})_{0.98}O_3$ relaxor ferroelectric ceramic by Selvamani *et al*.[23] They have observed a temperature change of 0.06 K with 1 kV $mm^{-1}$ at room temperature. The morphotropic phase boundary (MPB) composition $PbZr_{0.52}Ti_{0.48}O_3$[20] as well is used as capacitors due to their high dielectric constants.[24] However, applications of $PbZr_{0.52}Ti_{0.48}O_3$-based ceramics in cooling purposes have not been contemplated.

The modern refrigeration demands those materials which show ECE at easily achievable temperatures, particularly near room temperature. The reason behind choosing the doping of $Bi^{3+}$ at $Pb^{2+}$ is, it lowers the transition temperature of

‡Corresponding author.

PZT from 450°C to 395°C.[25,26] Moreover, the substitution of Bismuth in PZT at MPB enhances the ferroelectric properties, diffuses the phase transition and hence provides wide industrial applications.[25,26] So, we have planned to study the ECE in Bi-doped PZT at MPB composition by optimizing the sintering temperature. Henceforth, an organized inquiry on structural, microstructure, ferroelectric and electrocaloric properties of $(Pb_{0.8}Bi_{0.2})(Zr_{0.52}Ti_{0.48})O_3$ have been carried out. Moreover, the thermal energy conversion using Olsen cycle has been investigated.

## 2. Materials and Methods

### 2.1. *Materials*

The $(Pb_{0.8}Bi_{0.2})(Zr_{0.52}Ti_{0.48})O_3$ powder was synthesized from metal oxide using conventional solid-state reaction technique. The PbO, $Bi_2O_3$, $ZrO_2$, $TiO_2$ (99.9%) from Sigma Aldrich were used as resources. All the raw metal oxides were weighed accordingly and blended using mortar and pestle. The powder was then ball milled uninterruptedly in a bottle comprising propanol and zirconia balls for 24 h. Afterward, the mixed powder was heat treated at 900°C for 4 h followed by mixing of PVA (2 weight %) binder. After this, cylindrical-shaped discs of 10 mm diameter and 1 mm thickness were made with the help of a hydraulic press. These pellets were sintered at 1000°C, 1050°C, 1100°C and 1150°C for 2 h in lead environs to lessen the emaciation due to the elusiveness of lead. This temperature range and sintering time have been decided by the initial trial study. The samples sintered at 1000°C, 1050°C, 1100°C and 1150°C have represented as S1–S4, respectively, throughout.

### 2.2. *Methods*

The X-Ray diffraction (XRD) data of all the sintered samples were taken from 10° to 70° at a scan speed of 2°/min with CuK$\alpha$ ($\lambda$ = 1.54 Å) anode. The Rietveld refinement of the experimental data has been done using FULLPROF SUITE SOFTWARE. The parameters which were taken for the refinement purpose are lattice parameters, zero displacements, scale factors, atomic position of Zr/Ti, O (OI and OII). The peak profile of data was modeled with the use of the Pseudo–Voigt function with axial divergence symmetry. The background was fitted with the help of sixth-order polynomial. The surface morphology was inquired using Field Emission Scanning Electron Microscope (FE-SEM), Supra 55 from Carl Zeiss. All the micrographs were set down at the same magnification of 15KX using In-Lens detector. The grain size was calculated using 'Image J' software. The total of 100 grains is taken for the calculation of grain size for each sample. The density of all the sintered samples was measured with the help of lab made setup based on Archimedes Principle. The automatic PE loop tracer from Marine India was used to measure the ferroelectric properties. The size and thickness of the electrode are maintained the same for each sample for the accurate comparison of polarization.

The primary investigation of ECE was done by using the direct method with the help of an IR thermometer. The exact value of ECE was calculated by an indirect method based on Maxwell's relation of entropy ($S$) and Polarization ($P$) given in the following equation:

$$\left(\frac{\partial P}{\partial T}\right)_E = \left(\frac{\partial S}{\partial E}\right)_T. \tag{1}$$

The adiabatic reversible temperature change ($\Delta T$) of a material having density ($\rho$) and heat capacity ($C$) can be calculated by using Eq. (2),

$$\Delta T = -\frac{1}{\rho}\int_{E_1}^{E_2}\frac{T}{C}\left(\frac{\partial P}{\partial T}\right)_E dE. \tag{2}$$

Values of $\frac{\partial P}{\partial T}$ were obtained from the third or fourth-order polynomial which best fits to Polarization ($P$) versus Temperature ($T$) profile. The heat capacity $C = 0.32194$ $Jg^{-1}$ $K^{-1}$ remains sensibly constant for Zr rich ceramics in the temperature range of interest.[10] The lower and higher integration limit ($E_1$ and $E_2$, respectively) and temperature regions for all the samples have been deliberately chosen to obtain the consistent data set. When an electric field is directly applied at the two poles of the sample; the dipolar entropy of the sample decreases. This is due to the reason that the electric dipoles rearrange themselves in the direction of the applied field and hence the degree of ordering increases. This leads to the overall rise in the temperature of the sample. Though, the excess amount of heat is observed and controlled by the temperature controller to sustain the temperature of the sample. On the other hand, when the external field is detached from the system, the dipoles re-attain their original positions and the overall dipolar entropy increases along with the instantaneous decrease in net temperature.[27] For the theoretical calculations, Landau's phenomenological approach has been used.

The high-field thermal energy conversion was calculated from ferroelectric loops using the Olsen cycle. The Olsen cycle suggested by Olsen *et al*. resembles to Ericson cycle, which can be used to generate electricity with the help of high-field pyroelectric effect.[5,6,28,29] The high-conversion efficiency (upto 37.5%) of the Carnot cycle permits by the Olsen cycle which consists of 2 isothermal and 2 isoelectric field operations.[30] The area swept by the Olsen cycle gives the value of the energy conversion density of the material. A more intense discussion about the Olsen cycle is available in many articles.[6,29,30] The energy conversion density has been calculated by

$$W = \int_{P_r}^{P_{\max}} EdP, \tag{3}$$

where $W$ represents the energy conversion density in the material; $E$ is the applied electric field; $P_r$ and $P_{\max}$ are remnant and maximum polarization, respectively.

## 3. Results

### 3.1. *XRD analysis*

The XRD data for all the samples have been recorded and analyzed. The X-Ray diffractograms of S1–S4 (names as given in Sec. 2.1) are shown in Fig. 1. The visual analysis of diffractograms reveals variation in reflections present near 38.3° and 44.5° (shown in Fig. 2). In samples S1 and S2, the reflection peak at 38.3° is singlet whereas the peak at 44.5° shows doublet behavior which give indication toward the distorted perovskite structure like tetragonal (as the base material PZT has a tetragonal structure). Further splitting in these peaks in samples S3 and S4 designate a change in structure than tetragonal. For the conclusive analysis, the Rietveld refinement has been done using various structure models.

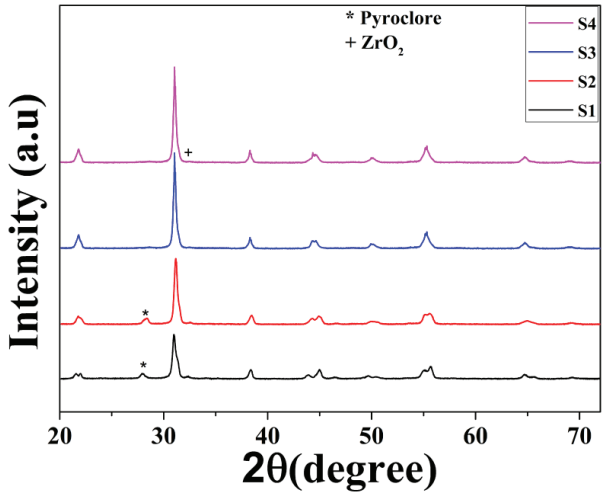


Fig. 1. X-Ray diffractograms of S1–S4.

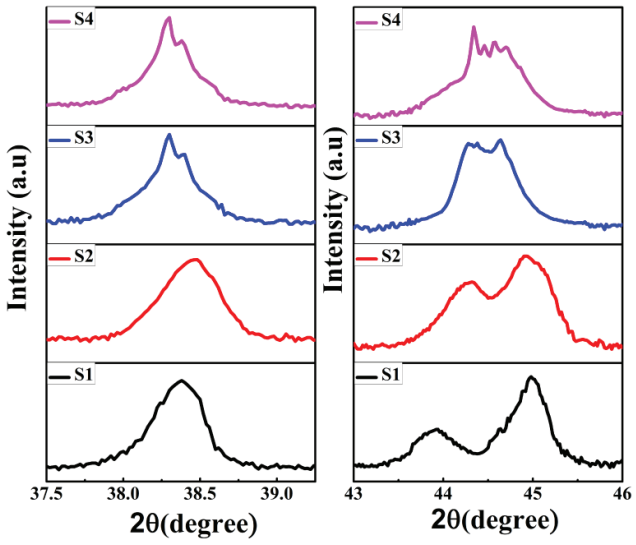


Fig. 2. Variation in the diffraction peaks at 38.3° and 44.5°.

For samples S1 and S2, the initial tetragonal structural model was supposed to be very comparable to crystallography open database (COD) ID 1526147.[31] In this phase, Pb/Bi were placed at Wyckoff's site 1a (0, 0, 0), Zr/Ti at 1b (0.5, 0.5, $z$), OI at 1b (0.5, 0.5, $z$) and OII at 2c (0.5, 0, $z$), where $z$ represents the refineable parameter. For samples S3 and S4, additional phases along with the tetragonal phase have been intensively investigated. It has been found that the monoclinic phase in addition to the tetragonal phase shows the best fit with experimental data. The monoclinic phase has been assumed to be close to COD ID 1526149.[31] In this phase, the Pb/Bi ion was placed at Wyckoff's site 2a (0, 0, 0), Zr/Ti at 2a ($x$, 0, $z$), OI at 2a ($x$, 0, $z$) and OII at 4b ($x$, $y$, $z$), where $x$, $y$ and $z$ represents the refineable parameters. The refined XRD patterns for all the samples are shown in Fig. 3. It can be clearly seen from the refined data that the samples S1 and S2 show a good fit with tetragonal phase having P4mm symmetry along with some pyrochlore as impurity phase. Whereas the refinement of samples S3 and S4 show very good agreement with mixed phase (tetragonal and monoclinic). In addition to this, an impure phase of unreacted $ZrO_2$ is present in S4 which may be due to the volatilization of lead at higher temperature. It has been found that goodness of fitting (GOF) for all the samples lies under five which proves a very good hormonal between experimental and theoretical data.

The refined parameters for all the samples are listed in Table 1. It is very interesting to observe that the different sintering temperatures significantly affect the same composition. Hence, from the XRD analysis, sintering temperature 1100°C (sample S3) seems to be the optimum temperature to get MPB with no considerable traces of impurity phase.

### 3.2. *Microstructure analysis and density measurement*

The scanning electron micrographs of all the samples from S1 to S4 are shown in Fig. 4. A gradual increase in grain size from samples S1 to S3 followed by a decrease for S4 is clearly seen from the images. The average grain size values for samples S1–S4 are 0.75, 1.05, 2.70 and 1.70 $\mu$m, respectively. Comparatively high grain size, opaque surface structure along with clear boundary limits suggests the good quality of S3 sample.

The density of all the samples is in increasing order from S1 to S3 then decreases for S4. The values of experimentally measured density are 5.49, 6.14, 7.06 and 6.25 g cm$^{-3}$, respectively, for samples S1–S4. Thus, the data collected from density measurements also matches quite well with the FE-SEM records. With the rise in sintering temperature, the grain size increases due to which grains become tightly packed leading to an increase in density value. The reason behind the decrease in grain size and density for S4 is the volatility of lead which has been confirmed in XRD analysis. Due to the loss of lead at high temperature that is for sample S4, an un-reacted $ZrO_2$ impurity phase appears (as shown in Fig. 1). This causes

Table 1. Refined parameters of XRD data for samples S1–S4.

| Sample | S1 | S2 | S3 | | S4 | |
|---|---|---|---|---|---|---|
| Space group | P4mm (tetragonal) | P4mm (tetragonal) | P4mm (tetragonal) | C1m1 (monoclinic) | P4mm (tetragonal) | C1m1 (monoclinic) |
| *a* (Å) | 4.03 | 4.03 | 4.0558 | 5.7695 | 4.0609 | 5.7058 |
| *b* (Å) | 4.03 | 4.03 | 4.0558 | 5.7687 | 4.0609 | 5.7585 |
| *c* (Å) | 4.12 | 4.09 | 4.0895 | 4.0502 | 4.0828 | 4.1027 |
| *β* (deg) | 90 | 90 | 90 | 90.388 | 90 | 90.381 |
| Zr/Ti | 0.5/0.5/0.44 | 0.5/0.5/0.45 | 0.5/0.5/0.42 | 0.523/0/0.44 | 0.5/0.5/0.4515 | 0.5330/0/0.42 |
| OI | 0.5/0.5/0.68 | 0.5/0.5/0.65 | 0.5/0.5/−1.91 | 0.5515/0/0.028 | 0.5/0.5/1.0211 | 0.5412/0/0.01 |
| OII | 0.5/0/0.068 | 0.5/0/0.08 | 0.5/0/0.68 | 0.2880/0.2434/0.03 | 0.5/0/0.3927 | 0.2692/0.2314/0.04 |
| Phase fraction | 100 | 100 | 68 | 32 | 69 | 31 |
| V (Å$^3$) | 67.098 | 66.60 | 67.27 | 134.79 | 67.32 | 134.80 |
| $R_{wp}$ | 5.0 | 5.43 | 6.11 | | 5.89 | |
| $\chi^2$ | 4.1 | 4.09 | 1.61 | | 2.83 | |

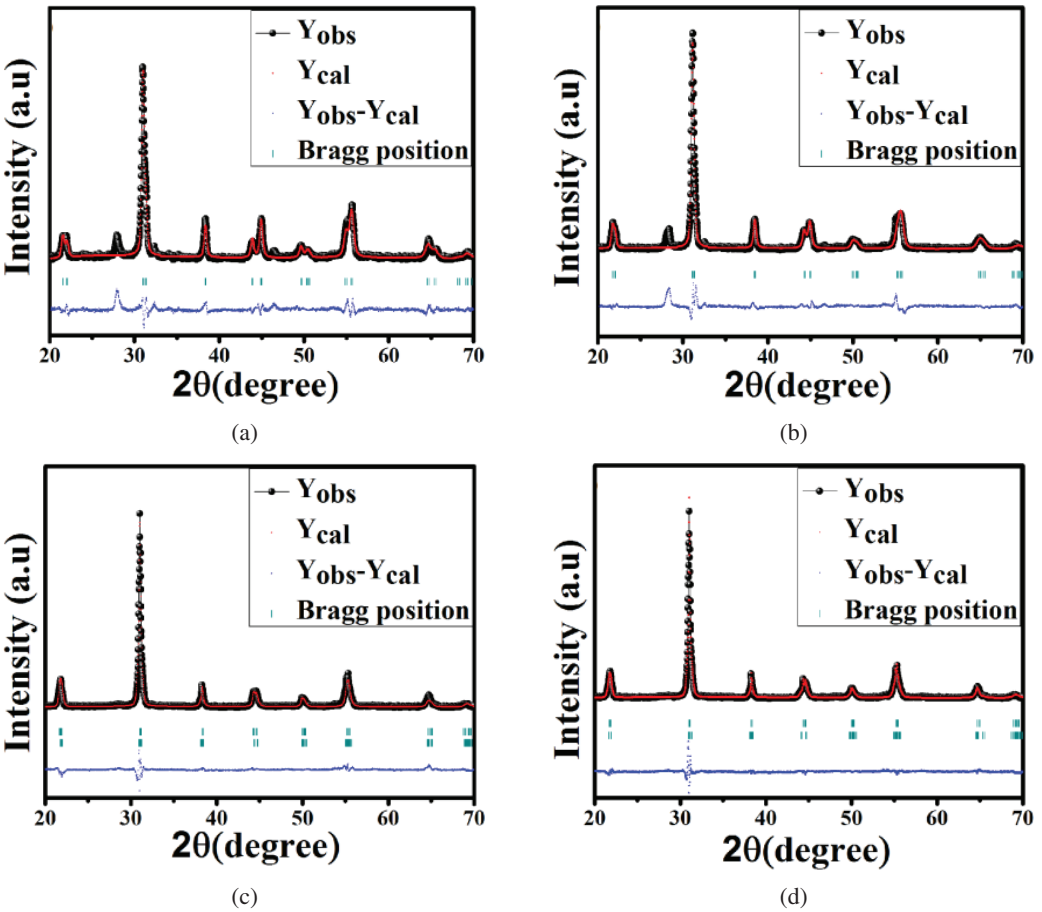


Fig. 3. Refined XRD pattern for (a) S1, (b) S2, (c) S3 and (d) S4 samples.

strain in the system and may lead to a decrease in the grain size. The calculated value of experimental density, theoretical density, grain size and standard deviation in grain size for all the samples are given in Table 2. Also, the trend of calculated value of grain size and experimental density is shown in Fig. 5.

### 3.3. *Ferroelectric properties*

Figure 6(a) shows room temperature hysteresis loops for all the samples. The ferroelectric polarization in all the samples is apparently due to the hybridization in 3*d* and 2*p* states of titanium and oxygen ion.[32] A gradual increase in remnant

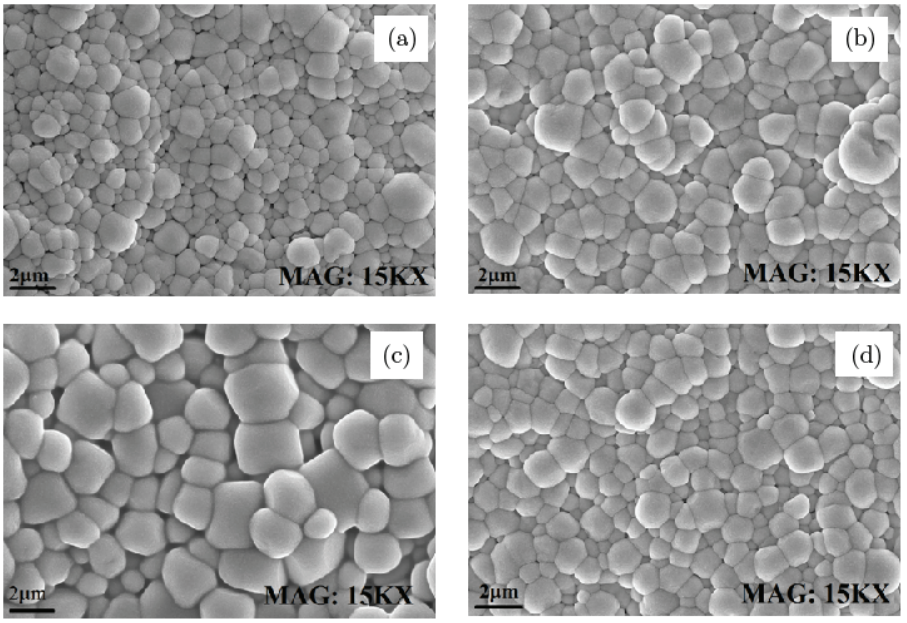


Fig. 4. Scanning electron micrographs of (a) S1, (b) S2, (c) S3 and (d) S4 samples.

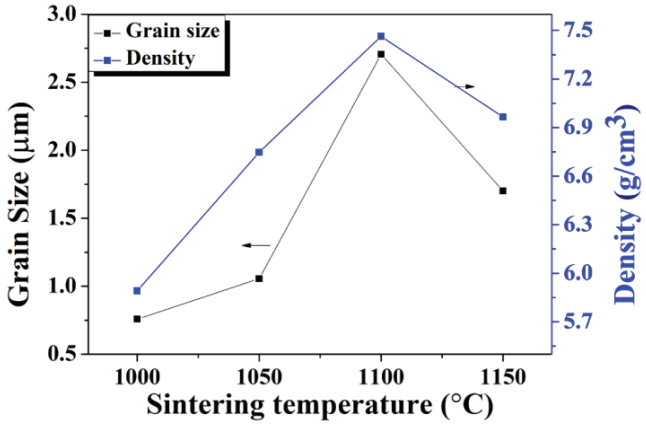


Fig. 5. The trend of the calculated value of grain size and experimental density.

Table 2. Calculated value of grain size and experimental density of all the samples.

| Sample | Experimental density (g cm$^{-3}$) | Theoretical density (g cm$^{-3}$) | Grain size ($\mu$m) | Standard deviation |
|---|---|---|---|---|
| S1 | 5.49 | 5.55 | 0.75 | 0.21 |
| S2 | 6.14 | 6.23 | 1.05 | 0.19 |
| S3 | 7.06 | 7.19 | 2.72 | 0.11 |
| S4 | 6.25 | 6.60 | 1.70 | 0.26 |

polarization ($P_r$) upto S3 and a decrease afterward can be easily seen from Fig. 6(b). Also, the values of the coercive field for all the samples are different. There are two main reasons behind significant high values of $P_r$ in samples S3 and S4. First is the increase in grain size leading to a decrease in grain boundaries which results in enhanced ferroelectric properties of these samples.[33] Other is the presence of MPB in these samples as ferroelectric polarization changes crystallography directions from one phase to another at MPB.[31,34] Furthermore, this strong ferroelectric behavior can also be justified by the presence of $Bi^{3+}$ ions in PZT.[35] Henceforth, the samples S3 and S4 by having maximum values of $P_r$ are prioritized for the next step to examine the ferroelectric behavior at higher temperature. In both the S3 and S4 samples, due to the presence of double phase, the polarization increases, however, due to the loss of lead at a higher temperature, its value decreases in S4 than S3 but still greater than all other samples. Besides, due to the contribution of both the phases that are tetragonal and rhombohedral, less energy is required to polarize the material, hence softening of the material has been take place.

The polarization ($P$) versus electric field ($E$) profile at different temperatures has been recorded and examined. Figure 7 shows $P$ versus $E$ loops of samples S3 and S4 at frequency 50 Hz and at field 35 kV/cm. A back switching has been observed with an increase in temperature. The reduction in internal stress with rise in temperature is responsible for this back switching in ferroelectric material.[36–38]

### 3.4. *Experimental measurements of ECE*

The polarization versus temperature profiles at four different electric field values (5, 10, 15 and 20 kV cm$^{-1}$) is shown in Fig. 8. These polarization values have been calculated from the upper branches of $P$ versus $E$ loops using the method offered in the literature.[10] The trends of $\Delta T$ versus $T$ for

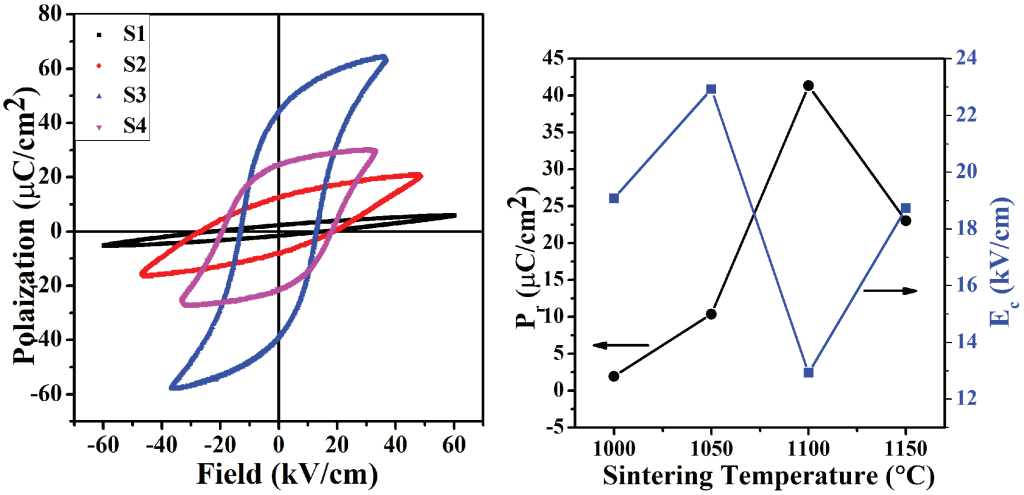


(a) (b)

Fig. 6. (a) Room temperature hysteresis loops at different sintering temperature and (b) remnant polarization and coercive field versus sintering temperature profile.

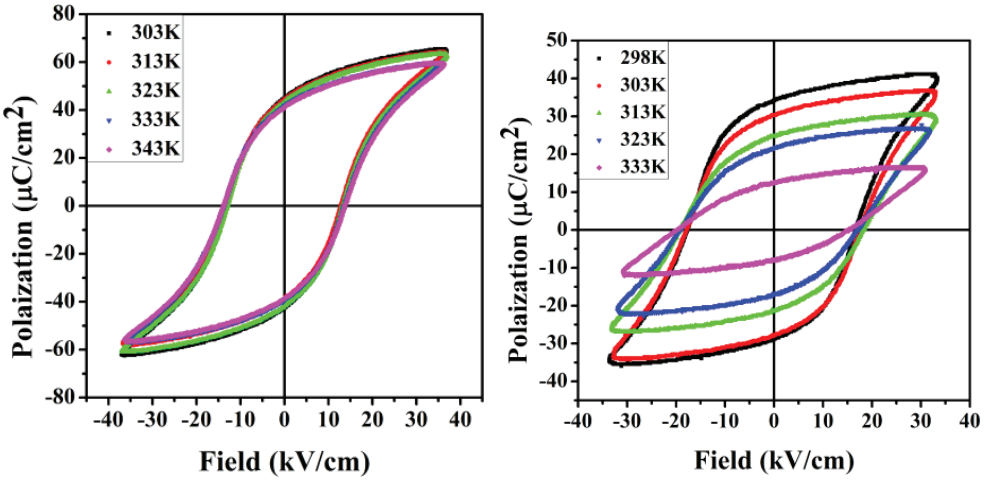


(a) (b)

Fig. 7. *P-E* loops at different temperatures for (a) S3 and (b) S4 samples.

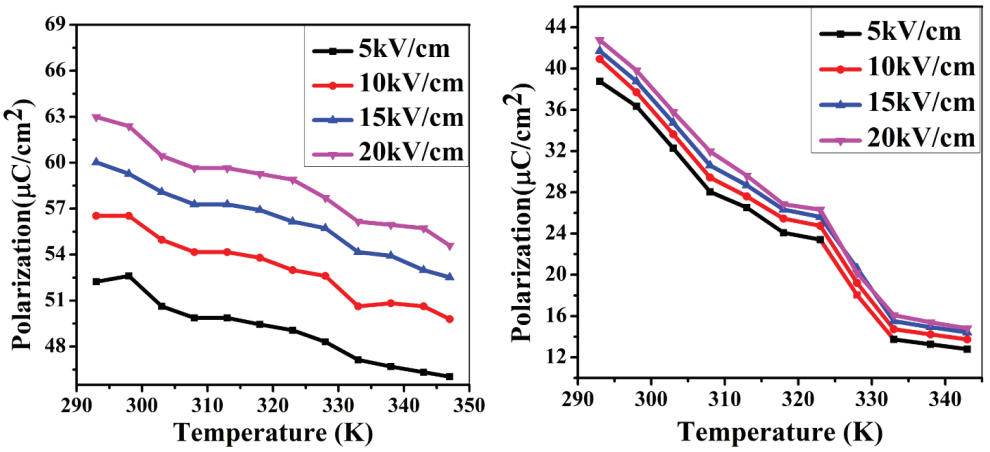


(a) (b)

Fig. 8. Polarization versus temperature plots of (a) S3 and (b) S4 samples.

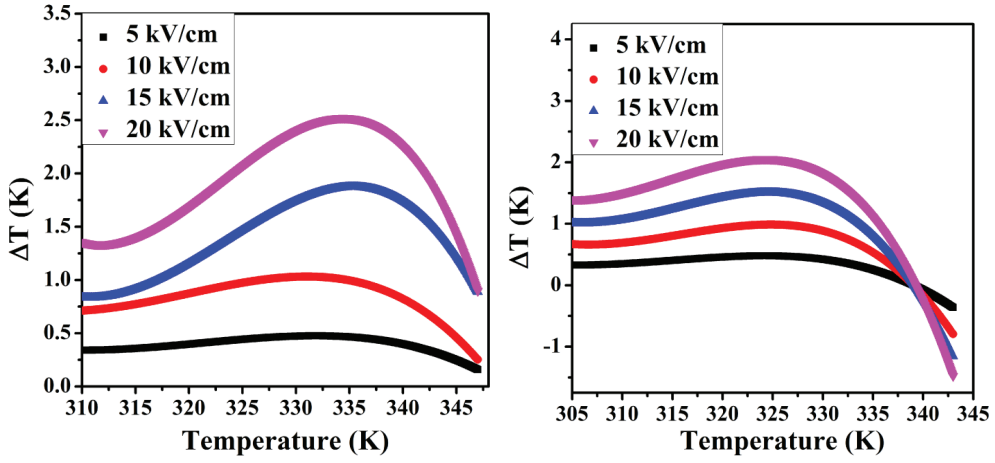


Fig. 9. EC temperature change for (a) S3 and (b) S4 samples.

samples S3 and S4 which obtained with the help of Eq. (2) are given in Fig. 9. An increase in $\Delta T$ with the increase in electric field is clearly visible for both the samples. Moreover, Fig. 9 reveals that external temperature has a great influence on the temperature change of the sample itself.[39–41] The peak values of $\Delta T$ at 20 kV cm$^{-1}$ have been observed to be 2.53 K and 2.04 K for samples S3 and S4, respectively. The value of $\Delta T$, electrocaloric strength ($\zeta$), and the temperature at which the maximum $\Delta T$ occurs ($T_{max}$) for both the samples are listed in Table 3. Besides, the large change in the temperature values ($\Delta T$) appears due to the large entropy change (as shown in Fig. 10) that comes from the induced ordering of random domains on the application of the electric field. A comparison of $\zeta$ in bulk ferroelectrics is given in Table 4. Comparatively, a high value of strength is validated by the strong ferroelectric properties of the prepared sample. However, the microscopic mechanism behind the ECE has not been established yet. At this stage, sample S3 has been chosen for further calculations as it has shown the highest electrocaloric strength.

Table 3. Value of temperature change ($\Delta T$), EC strength ($\zeta$), and the temperature at which the maximum $\Delta T$ occurs ($T_{max}$) for (a) S3 and (b) S4 samples.

| Sample | $\Delta T$ (K) | $\zeta$ (K mm/kV) | $T_{max}$ (K) |
|---|---|---|---|
| S3 | 2.53 | 1.26 | 335 |
| S4 | 2.04 | 1.02 | 325 |

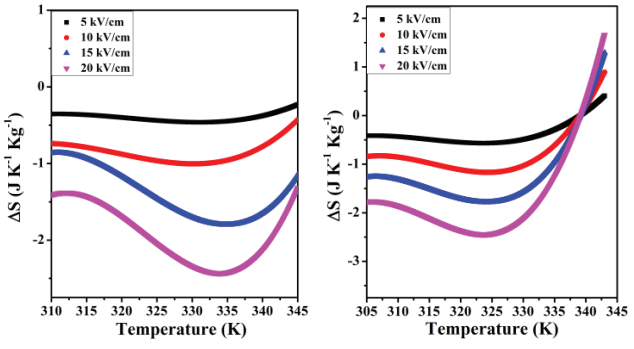


Fig. 10. $\Delta S$ versus temperature profile for samples (a) S3 and (b) S4.

### 3.5. *Theoretical calculation for ECE*

The authenticity of experimentally obtained results has been inspected by applying the phenomenological approach of ECE on sample S3. According to this theory, the entropy of a system $S(E, T)$ can be represented as a sum of two components:

$$S(E, T) = S_{latt}(T) + S_{dip}(E, T), \tag{4}$$

where $S_{latt}(T)$ is the entropy of weakly polarizable lattice and $S_{dip}(E, T)$ is the contribution of the dipolar part. The dipolar degree of freedom in ferroelectrics is associated with individual dipolar moments. Since a system investigated for ECE involves adiabatic changes which imply that total change of entropy $\Delta S(E, T)$ must be zero, Eq. (4) becomes

$$0 = \Delta S_{latt}(T) + \Delta S_{dip}(E, T). \tag{5}$$

An adiabatically application of electric field results in an increase in temperature of material due to an increase in lattice vibration. In order to maintain Eq. (4), compensational reduction in dipolar entropy occurs. On the other hand, adiabatically removal of the electric field leads to decrease in temperature of material as lattice vibration decreases and hence dipolar entropy increases. The Change in dipolar entropy is responsible for the ECE in a material, as the adiabatic temperature change $\Delta T$ is calculated from $\Delta S_{dip}(E, T)$,

$$\Delta T = \frac{T\Delta S_{dip}(E,T)}{C}, \tag{6}$$

Table 4. Comparison of electrocaloric strength in bulk ferroelectrics.

| Material | $\Delta T$ (K) | $E$ (kV/cm) | $\zeta$ (K cm/kV) | Reference |
|---|---|---|---|---|
| $Pb(Zr_{0.75}Sn_{0.20}Ti_{0.05})O_3$ | 2.5 | 30 | 0.08 | 7 |
| $(PbZrO_3)_{0.71}(BaTi_{03})_{0.29}$ | 0.15 | 20 | 0.008 | 9 |
| $Pb(Zr_{0.455}Sn_{0.455}Ti_{0.09})O_3$ | 0.6 | 30 | 0.02 | 9 |
| $0.92(Na_{0.5}Bi_{0.5})TiO_3$–$0.08BaTiO_3$ | 0.2 | 40 | 0.005 | 20 |
| PLZT (8/65/35) | 0.26 | 10 | 0.026 | 23 |
| 0.70PMN-0.30PT | 2.7 | 12 | 0.225 | 42 |
| PMN-PT 90/10 single crystal | 1 | 40 | 0.025 | 43 |
| $Ba_{0.65}Sr_{0.35}TiO_3$ | 0.23 | 10 | 0.023 | 44 |
| BZT-BCT | 0.04 | 12 | 0.003 | 45 |
| $BaSn_{0.12}Ti_{0.88}O_3$ | 0.27 | 10 | 0.027 | 46 |
| GdNBT | 0.75 | 90 | 0.008 | 47 |
| PLZT | 0.26 | 30 | 0.086 | 48 |
| $Pb_{0.97}La_{0.02}(Zr_{0.95}Ti_{0.05})_{1\text{-}0.01}O_3$ | −12.45 | 50 | 0.249 | 49 |
| $Pb_{0.97}La_{0.02}(Zr_{0.95}Ti_{0.05})\ O_3$ | −7.47 | 50 | 0.149 | 50 |
| $Pb_xSr_{1-x}TiO_3$, $x = 0.35$ | 2.05 | 40 | 0.051 | 51 |
| $Ba_xSr_{1-x}TiO_3$, $x = 0.35$ | 0.49 | 50 | 0.009 | 52 |
| BNT-6BT | 1.1 | 25.24 | 0.043 | 53 |
| $BaTi_{0.89}Sn_{0.11}O_3$ | 0.71 | 25 | 0.0284 | 54 |
| $(Pb_{1-x}Bi_x)(Zr_{0.52}Ti_{0.48})O_3$, $x = 0.2$ | 2.536 | 20 | 0.1268 | This work |

where $C$ is the heat capacity. $\Delta S_{\text{dip}}(E, T)$ can be calculated using the relation $\Delta S_{\text{dip}}(E,T) = -\left(\frac{\partial G}{\partial T}\right)_E$, where $G$ is the Gibbs free energy. According to the phenomenological theory of ECE, the free energy of ferroelectric material can be derived in terms of electric polarization

$$G = G_o + \frac{1}{2}\beta(T - T_c)P^2 + \frac{1}{4}\xi P^4 - EP, \tag{7}$$

where $G_o$ is the free energy of paraelectric phase, $\beta(\varepsilon_o c)^{-1}$, where $c$ = curie constant) and $\xi$ are temperature independent phenomenological coefficients and $T_c$ is curie temperature. By differentiating Eq. (7), dipolar entropy change is obtained as $\Delta S_{\text{dip}}(E,T) = -\frac{1}{2}\beta P^2$ which is used in Eq. (6) to get $\Delta T$,

$$\Delta T = -\frac{T\beta P^2}{2C}. \tag{8}$$

By differentiating G (Eq. (7)) with respect to $P$ and applying $dG/dP = 0$, we get

$$E = \beta(T - T_c)P + \xi P^3. \tag{9}$$

At zero field that is $E = 0$,

$$P^2 = \beta(T_c - T)/\xi. \tag{10}$$

Further differentiation of Eq. (9) with respect to $P$ results in reciprocal permittivity,

$$\frac{1}{\varepsilon} = \beta(T - T_c) + 3\xi P^2, \tag{11}$$

with the use of Eqs. (10) and (11), permittivity versus temperature profile (given in Fig. 11) and $P$ versus $E$ loops at different temperatures, $\beta$ and $\xi$ can be easily evaluated.

From Eqs. (8) to (10), after using obtained values of $\beta$ and $\xi$, we get that

$$\Delta T = -\frac{T\beta}{2C}\left(\frac{E}{2\xi}\right)^{2/3}. \tag{12}$$

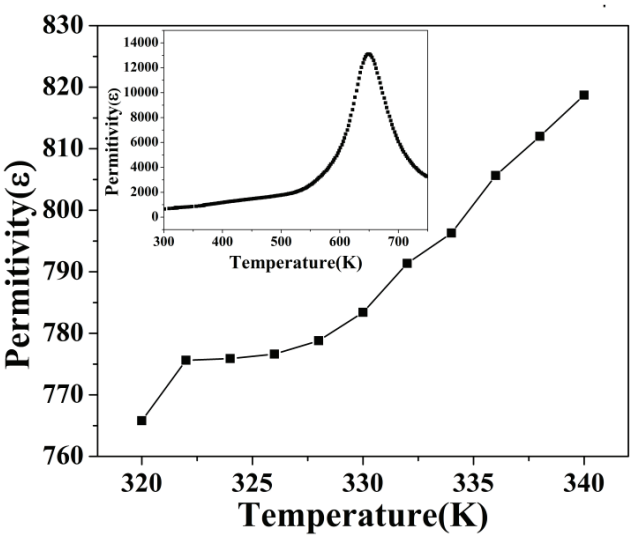


Fig. 11. Permittivity versus temperature profile (dielectric properties for sample S3).

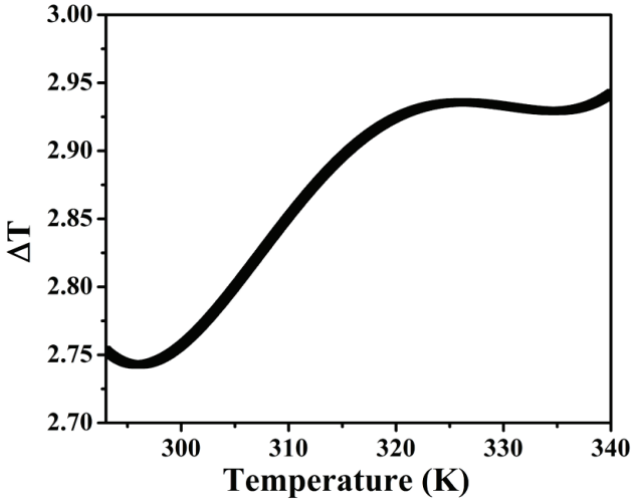


Fig. 12. Temperature change under an electric field 20 kV/cm for sample S3.

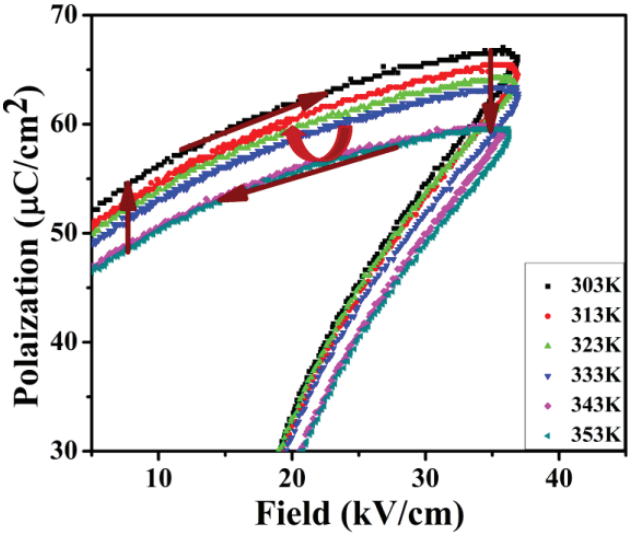


Fig. 13. Olsen cycle applied on sample S3.

Based upon the above equation the temperature change under an electric field 20 kV/cm for sample S3 is shown in Fig. 12. The calculated value of temperature change at 335 K is approximately 2.92 K which is very close to the experimentally obtained value (2.53 K).

### 3.6. *Thermal energy conversion*

Olsen cycle has been applied on the sample S3 as shown in Fig. 13. With the help of Eq. (3), the value of energy conversion density has been calculated successfully. The lower value of the applied field and external temperature are kept constant at 0 kV/cm and 30°C, respectively. Figure 14 gives the energy conversion density as a function of the applied field. It has been analyzed from results that the value of energy density

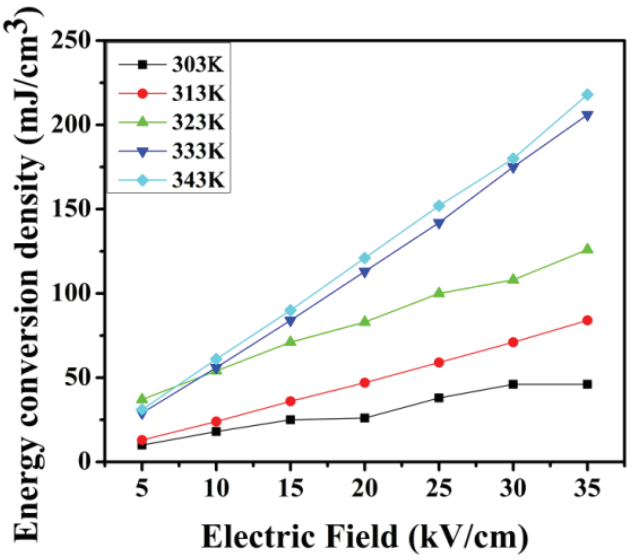


Fig. 14. Energy conversion density as a function of higher applied field at different temperatures.

increases with an increase in both temperature and applied field. This is due to the fact that with the increase in electric field, polarization increases. Likewise, decrease in the maximum polarization with increase in temperature of material (i.e., ECE) also governs this response of energy density. The maximum value of energy conversion acquired for the Olsen cycle having parameters 30–70°C and 0–35 kV $cm^{-1}$ is 218 mJ $cm^{-3}$. A comparison of energy conversion density based upon the Olsen cycle in bulk ferroelectric materials is given in Table 5. For the comparison purpose, we have chosen only those materials which can be used for practical applications. Obviously, it is clear from the table that the prepared sample has relatively large energy conversion potential in small electric field and temperature ranges and hence exhibits promising thermal energy harvesting value.

## 4. Discussion

$Bi^{3+}$ by having a similar electronic configuration and compatible ionic radii as $Pb^{2+}$ has exhibited an enormous high value of polarization. Due to tremendous ferroelectric properties of $Bi^{3+}$ doped $PbZr_{0.52}Ti_{0.48}O_3$, it has been predicted that it would possess an enhanced ECE. Although the sample has shown ferroelectric transition quite far from room temperature, we have successfully established the relationship of processing parameters such as sintering temperature to obtain the MPB of two phases at room temperature. The presence of MPB is accountable for the improved ferroelectric properties as well as enhanced ECE. The analogy of theoretically obtained value of ECE with one which has obtained from the experimental method gives the validation of achieved results. Additionally, a significant high value of thermal energy conversion has procured from conveniently attained working parameters which make this material available for practical applications.

Table 5. Comparison of Olsen cycle-based energy conversion density in bulk ferroelectric materials.

| Materials | Energy conversion ($kJ/m^3$) | Operating temperature range (°C) | Operating applied field range (kV/cm) | Reference |
|---|---|---|---|---|
| PZST | 100 | 146–159 | 0–29 | 27 |
| PZST | 131 | 157–177 | 4–32 | 55 |
| PMN-10PT | 186 | 30–80 | 0–35 | 2 |
| PMN-32PT | 100 | 80–170 | 2–9 | 56 |
| Hard PZT | 189 | 25–160 | 1–20 | 57 |
| PZN-4.5PT | 217 | 100–160 | 0–20 | 5 |
| Soft PZT | 92 | 25–160 | 1–20 | 57 |
| PZN-5.5PT | 150 | 100–190 | 0–12 | 6 |
| $K[(Nb_{0.90}Ta_{0.10})_{0.99}Mn_{0.01}]O_3$ | 629 | 120–160 | 1–50 | 58 |
| $Ba_{0.85}Sr_{0.15}Ti_{0.9}Zr_{0.1}O_3$ | 200 | 30–90 | 0–20 | 30 |
| $0.5Ba(Zr_{0.2}Ti_{0.8})O_3$-$0.5(Ba_{0.7}Ca_{0.3})TiO_3$ | 87 | 20–120 | 1–10 | 58 |
| BNT-BZT | 100 | 30–70 | 0–80 | 59 |
| $BaTi_{0.89}Sn_{0.11}O_3$ | 84.4 | 30–140 | 0–25 | 54 |
| $(Pb_{1-x}Bi_x)(Zr_{0.52}Ti_{0.48})O_3$, $x = 0.2$ | 218 | 30–70 | 0–35 | This work |

## 5. Conclusions

The ECE was explored for $(Pb_{0.8}Bi_{0.2})(Zr_{0.52}Ti_{0.48})O_3$ by optimizing the sintering temperature. Based upon XRD analysis, density and grain size measurements and ferroelectric performance, the sample sintered at 1100°C has chosen for the calculations of ECE and thermal energy conversion. This sample has experimentally exhibited the maximum adiabatic temperature change of 2.53 K with EC strength of 1.26 K mm $kV^{-1}$. Whereas an electrocaloric temperature change of 2.92 K has derived from phenomenological approach which is in close agreement with experimentally attained results. Furthermore, the energy conversion density of 218 mJ $cm^{-3}$ has obtained from the Olsen cycle having parameters 30–70°C and 0–35 kV $cm^{-1}$. Eventually, this study promotes the solid-state electrocaloric refrigeration and is helpful in the fabrication of micro-devices based upon the thermal energy conversion.

## Acknowledgments

The authors wish to thank the Centre for Emerging Life Sciences, GNDU for providing characterization facilities (FE-SEM). Author Shubhpreet Kaur also wishes to thank DEST SERB and Rusa-2.0 for providing financial support.

## References

[1]A. S. Bhalla, R. Guo and R. Roy, The perovskite structure — A review of its role in ceramic science and technology, *Mater. Res. Innov.* **4**, 3 (2000).

[2]G. Sebald, S. Pruvost and D. Guyomar, Energy harvesting based on Ericsson pyroelectric cycles in a relaxor ferroelectric ceramic, *Smart Mater. Struct.* **17**, 015012 (2007), doi:10.1088/0964-1726/17/01/015012.

[3]C. B. Fleddermann and J. A. Nation, Ferroelectric sources and their application to pulsed power: A review, *IEEE Trans. Plasma Sci.* **25**, 212 (1997).

[4]S. Zhang, F. Li, X. Jiang, J. Kim and J. Luo, Progress in materials science ferroelectric crystals for electroacoustic transducers — A review, *Prog. Mater. Sci.* **68**, 1 (2015).

[5]A. Khodayari, S. Pruvost, G. Sebald, D. Guyomar and S. Mohammadi, Nonlinear pyroelectric energy harvesting from relaxor single crystals, *IEEE Trans. Ultrason. Ferroelectr. Freq. Control* **56**, 693 (2009).

[6]F. Y. Lee, S. Goljahi, I. M. Mckinley, C. S. Lynch and L. Pilon, Pyroelectric waste heat energy harvesting using relaxor ferroelectric 8/65/35 PLZT and the Olsen cycle, *Smart Mater. Struct.* **21**, 12 (2012).

[7]B. A. Tuttle and D. A. Payne, The effects of microstructure on the electrocaloric properties of $Pb(Zr,Sn,Ti)O_3$ ceramics, *Ferroelectrics* **37**, 603 (1981).

[8]W. N. Lawless, Specific heat and electrocaloric properties of $KTaO_3$ at low temperatures, *Phys. Rev. B* **16**, 433 (1977).

[9]P. D. Thacher, Electrocaloric effects in some ferroelectric and antiferroelectric $Pb(Zr, Ti)O_3$ compounds, *J. Appl. Phys.* **39**, 1996 (1968).

[10]A. S. Mischenko, Q. Zhang, J. F. Scott, R. W. Whatmore and N. D. Mathur, Giant electrocaloric effect in thin-film $PbZr_{0.95}Ti_{0.05}O_3$, *Science* **311**, 1270 (2006).

[11]D. Saranya, A. R. Chaudhuri, J. Parui and S. B. Krupanidhi, Electrocaloric effect of PMN-PT thin films near morphotropic phase boundary, *Bull. Mater. Sci.* **32**, 259 (2009).

[12]B. Neese, S. G. Lu, B. Chu and Q. M. Zhang, Electrocaloric effect of the relaxor ferroelectric poly(vinylidene fluoride-trifluoroethylene-chlorofluoroethylene) terpolymer, *Appl. Phys. Lett.* **94**, 042910 (2009).

[13]S. G. Lu *et al.*, Organic and inorganic relaxor ferroelectrics with giant electrocaloric effect, *Appl. Phys. Lett.* **97**, 162904 (2010).

[14]T. M. Correia *et al.*, Investigation of the electrocaloric effect in a $PbMg_{2/3}Nb_{1/3}O_3$-$PbTiO_3$ relaxor thin film, *Appl. Phys. Lett.* **95**, 20 (2009).

[15]R. Pirc, Z. Kutnjak, R. Blinc and Q. M. Zhang, Electrocaloric effect in relaxor ferroelectrics. *J. Appl. Phys.* **110**, 074113 (2011).

[16]Z. Kutnjak, B. Rožič and R. Pirc, Electrocaloric effect: Theory, measurements, and applications, Wiley encyclopedia of electrical and electronics engineering, (2015), pp. 1–19, doi:10.1002/047134608X.W8244.
[17]C. O. Paiva-Santos *et al.*, Effect of niobia on the crystal structure and dielectric characteristics of $Pb(Zr_{0.45}Ti_{0.55})O_3$ prepared from polymeric precursor, *Mater. Res. Bull.* **35**, 15 (2000).
[18]M. S. J. Nunes *et al.*, Microstructural and ferroelectric properties of $PbZr_{1-x}Ti_xO_3$ thin films prepared by the polymeric precursor method, *Mater. Lett.* **49**, 365 (2001).
[19]C. R. Cho, L. F. Francis and D. L. Polla, Ferroelectric properties of sol–gel deposited $Pb(Zr,Ti)O_3/LaNiO_3$ thin films on single crystal and platinized-Si substrates, *Mater. Lett.* **38**, 125 (1999).
[20]Y. Bai, G. P. Zheng and S. Q. Shi, Abnormal electrocaloric effect of $Na_{0.5}Bi_{0.5}TiO_3$-$BaTiO_3$ lead-free ferroelectric ceramics above room temperature, *Mater. Res. Bull.* **46**, 1866 (2011).
[21]Q. Zhang and R. W. Whatmore, Improved ferroelectric and pyroelectric properties in Mn-doped lead zirconate titanate thin films, *J. Appl. Phys.* **94**, 5228 (2003).
[22]R. Lal, S. C. Sharma and R. Dayal, Piezoelectric characteristics of spraydried PZT ceramics modified by isovalent, supervalent and subvalent substitutions, *Ferroelectrics* **100**, 43 (1989).
[23]R. Selvamani, G. Singh and V. S. Tiwari, Electro-caloric effect in PLZT (8/65/35) ceramic, *AIP Conf. Proc.* **1447**, 1281 (2012).
[24]W. Y. Pan, C. Q. Dam, Q. M. Zhang and L. E. Cross, Large displacement transducers based on electric field forced phase transitions in the tetragonal $(Pb_{0.97}La_{0.02})$ $(Ti,Zr,Sn)O_3$ family of ceramics, *J. Appl. Phys.* **66**, 6014 (1989).
[25]R. Rai and S. Sharma, Structural and dielectric properties of (La, Bi) modified PZT ceramics, *Solid State Commun.* **129**, 305 (2004).
[26]T. A. Babu, K. V. Ramesh, V. R. Reddy and D. L. Sastry, Structural and dielectric studies of excessive $Bi^{3+}$ containing perovskite PZT and pyrochlore biphasic ceramics, *Mater. Sci. Eng. B* **228**, 175 (2018).
[27]A. Greco and C. Masselli, Electrocaloric cooling: A review of the thermodynamic cycles, materials, models, and devices, *Magnetochemistry* **6**, 67 (2020).
[28]R. B. Olsen *et al.*, Pyroelectric conversion cycle of vinylidene fluoridetrifluoroethylene copolymer, *J. Appl. Phys.* **57**, 5036 (1985).
[29]A. Navid and L. Pilon, Pyroelectric energy harvesting using Olsen cycles in purified and porous poly (vinylidene fluoride-trifluoroethylene) [P(VDF-TrFE)] thin films, *Smart Mater. Struct.* **20**, 025012 (2011).
[30]S. Patel, D. Sharma, A. Singh and R. Vaish, Enhanced thermal energy conversion and dynamic hysteresis behavior of Sr-added $Ba_{0.85}Ca_{0.15}Ti_{0.9}Zr_{0.1}O_3$ ferroelectric ceramics, *J. Mater.* **2**, 75 (2016).
[31]B. Noheda *et al.*, A monoclinic ferroelectric phase in the $Pb(Zr_{1-x}Ti_x)O_3$ solid solution, *Appl. Phys. Lett.* **74**, 2059 (1999).
[32]R. E. Cohen, Origin of ferroelectricity in perovskite oxides, *Nature* **358**, 136 (1992).
[33]V. R. Mudinepalli, L. Feng, W. Lin and B. S. Murty, Effect of grain size on dielectric and ferroelectric properties of nanostructured $Ba_{0.8}Sr_{0.2}TiO_3$ ceramics, *J. Adv. Ceram.* **4**, 46 (2015).
[34]D. Damjanovic, A morphotropic phase boundary system based on polarization rotation and polarization extension, *Appl. Phys. Lett.* **97**, 24 (2010).
[35]A. Garg and D. C. Agrawal, Effect of rare earth (Er, Gd, Eu, Nd and La) and bismuth additives on the mechanical and piezoelectric properties of lead zirconate titanate ceramics, *Mater. Sci. Eng. B, Solid-State Mater. Adv. Technol.* **86**, 134 (2001).
[36]Y. M. Kang and S. Baik, In situ high-temperature X-ray diffraction study on domain evolution in ferroelectric $(Pb,La)TiO_3$ epitaxial thin films, *J. Appl. Phys.* **82**, 2532 (1997).
[37]B. Peng, Z. Xie, Z. Yue and L. Li, Temperature-dependent polarization back-switching and dielectric nonlinearity in $PbZr_{0.4}Ti_{0.6}O_3$ ferroelectric thin films, *J. Appl. Phys.* **116**, 034109 (2014).
[38]M. Valant, Electrocaloric materials for future solid-state refrigeration technologies, *Prog. Mater. Sci.* **57**, 980 (2012).
[39]A. Peláiz-Barranco, J. Wang and T. Yang, Direct and indirect analysis of the electrocaloric effect for lanthanum-modified lead zirconate titanate antiferroelectric ceramics, *Ceram. Int.* **42**, 229 (2016).
[40]I. J. Roh *et al.*, Thickness-dependent electrocaloric effect in $Pb_{0.9}La_{0.1}Zr_{0.65}Ti_{0.35}O_3$ films grown by sol–gel process, *J. Electron. Mater.* **45**, 1057 (2016).
[41]X. Q. Liu, T. T. Chen, M. S. Fu, Y. J. Wu and X. M. Chen, Electrocaloric effects in spark plasma sintered $Ba_{0.7}Sr_{0.3}TiO_3$-based ceramics: Effects of domain sizes and phase constitution, *Ceram. Int.* **40**, 11269 (2014).
[42]R. Chukka *et al.*, Enhanced cooling capacities of ferroelectric materials at morphotropic phase boundaries, *Appl. Phys. Lett.* **98**, 2011 (2011).
[43]L. Luo *et al.*, Pyroelectric and electrocaloric effect of ⟨1 1 1⟩-oriented 0.9PMN–0.1PT single crystal, *J. Alloys Compd.* **509**, 8149 (2011).
[44]Y. Bai, X. Han, K. Ding and L. J. Qiao, Combined effects of diffuse phase transition and microstructure on the electrocaloric effect in $Ba_{1-x}Sr_xTiO_3$ ceramics, *Appl. Phys. Lett.* **103**, 16 (2013).
[45]G. Singh *et al.*, Electro-caloric effect in $0.45BaZr_{0.2}Ti_{0.8}O_3$-$0.55Ba_{0.7}Ca_{0.3}TiO_3$ single crystal, *Appl. Phys. Lett.* **102**, 082902 (2013).
[46]X. Zhang *et al.*, Large electrocaloric effect in $Ba(Ti_{1-x}Sn_x)O_3$ ceramics over a broad temperature region, *AIP Adv.* **5**, 047134 (2015).
[47]M. Zannen *et al.*, Electrocaloric effect and energy storage in lead free $Gd_{0.02}Na_{0.48}Bi_{0.5}TiO_3$ ceramic, *Solid State Sci.* **66**, 31 (2017).
[48]H. Maiwa, Electrocaloric and electromechanical properties of $(Pb,La)(Zr,Ti)O_3$ ceramics, *Ferroelectrics* **556**, 51 (2020).
[49]Z. H. Niu *et al.*, Giant negative electrocaloric effect in B-site non-stoichiometric $(Pb_{0.97}La_{0.02})(Zr_{0.95}Ti_{0.05})_{1+y}O_3$ anti-ferroelectric ceramics, *Mater. Res. Lett.* **6**, 384 (2018).
[50]Y. C. Zhao *et al.*, Giant negative electrocaloric effect in anti-ferroelectric $(Pb_{0.97}La_{0.02})(Zr_{0.95}Ti_{0.05})O_3$ ceramics, *ACS Omega* **4**, 14650 (2019), doi:10.1021/acsomega.9b02149.
[51]P. Z. Ge *et al.*, Composition dependence of giant electrocaloric effect in $Pb_xSr_{1-x}TiO_3$ ceramics for energy-related applications, *J. Materiomics* **5**, 118 (2019).
[52]P. Z. Ge *et al.*, Energy storage properties and electrocaloric effect of $Ba_{0.65}Sr_{0.35}TiO_3$ ceramics near room temperature, *J. Mater. Sci. Mater. Electron.* **29**, 1075 (2018).
[53]L. Li *et al.*, Electrocaloric effect in La-doped BNT-6BT relaxor ferroelectric ceramics, *Ceram. Int.* **44**, 343 (2018).
[54]S. Merselmiz *et al.*, High energy storage efficiency and large electrocaloric effect in lead-free $BaTi_{0.89}Sn_{0.11}O_3$ ceramic, *Ceram. Int.* **46**, 23867 (2020).
[55]R. B. Olsen, D. A. Bruno, J. M. Broscoe and J. Dullea, Cascaded pyroelectric energy converter, *Ferroelectrics* **59**, 205 (1984), doi:10.1080/00150198408240091.
[56]R. Kandilian, A. Navid and L. Pilon, The pyroelectric energy harvesting capabilities of PMN–PT near the morphotropic phase boundary, *Smart Mater. Struct.* **20**, 055020 (2011).
[57]S. Patel, A. Chauhan and R. Vaish, Electric-field-driven caloric effects in ferroelectric materials for solid-state refrigeration, *Energy Technol.* **4**, 417 (2016), doi:10.1002/ente.201500285.
[58]R. Sao, G. Vats and R. Vaish, A prime lead-free ferroelectric ceramic for thermal energy harvesting: $0.88Bi_{0.5}Na_{0.5}TiO_3$-.02Sr-$TiO_3$-$0.1Bi_{0.5}Li_{0.5}TiO_3$, *Ferroelectrics* **474**, 1 (2015).
[59]M. Shen *et al.*, High room-temperature pyroelectric property in lead-free BNT-BZT ferroelectric ceramics for thermal energy harvesting, *J. Eur. Ceram. Soc.* **39**, 1810 (2019).